DELINEATION OF SUBSTANTIA NIGRA PARS USING DTI-BASED TRACTOGRAPHY ON T1-WEIGHTED IMAGES

By

Evan Michael Gabuya Oculam

A capstone project submitted for
Graduation with University Honors

June 1st, 2020

University Honors
University of California, Riverside

APPROVED

_____
Dr. Xiaoping Hu
Department of Bioengineering

_____
Dr. Richard Cardullo, Howard H Hays Jr. Chair, University Honors

Abstract

The substantia nigra, a neurochemical center of the basal ganglia, can be separated into two parts: the neuromelaninic SN pars compacta (SNc), and the ferritin containing SN pars reticulata (SNr). However, current studies utilize inconsistent segmentations of the whole substantia nigra volume, resulting in irreplicable findings. In the present study, we utilize T1-weighted images and subsequent diffusion tensor imaging (DTI) based tractography from seed masks of a parcellated substantia nigra to confirm previous findings of regioselective connectivity from the two pars. Our target masks include the striatum, thalamus, globus pallidus, and putamen, regions that have shown spatially different connectivity profiles from each of the pars. Using a normalized connectivity paramter to measure relative connectivity between each of the substantia nigra pars and target masks with a subsequent single-factor ANOVA and post hoc Tukey's HSD test, we found that the SNc connectivity profile is significantly different than the SNr and overlap parcellations to all of the target masks. However, there was no significant difference between overlap regions and SNr, nor were there any significant differences in regioselectivity, showing similar connectivity values for anterior and posterior portions of the target masks. While this finding failed to confirm regioselectivity between substantia nigra pars, we hypothesize that using the cortex as a target mask, with limbic structures as waypoints, may show regioselectivity based on the specific seed masks of each substantia nigra pars.

Table of Contents

Acknowledgements

I would like to dedicate this to the person who helped me throughout my four years at UCR, Dr. Jason Langley. I am grateful for his patience and willingness to teach me about this subject, and I would not be here or accomplished other things outside of this research without his support and guidance. In addition, I would also like to thank Dr. Xiaoping Hu and Dr. Xu Chen for helping me get started in the beginning of my career, and who were both extremely patient when learning the ropes. This all would not be possible without the help from you two.

I would also like to dedicate this to my Senior Design team Brandon, Stephen, and David. Out of all the time we have spent together, and the things we have done, I am proud to not only call you my colleagues, but more importantly good friends. In addition, I would also like to thank Dr. Robert McKee for encouraging me to keep going and being a light of fairness and enthusiasm throughout this final year of the Class of 2020.

Introduction

The substantia nigra, basal ganglia within the midbrain, can be functionally and anatomically separated into two separate regions: the substantia nigra pars compacta (SNc) and the substantia nigra pars reticulata (SNr). Each subregion of the substantia nigra have different structural and neurological characteristics that have been determined through histological staining, where the SNc has been shown to have higher concentrations of neuromelanin than the SNr, whereas the SNR has a corresponding higher concentration of iron compared to the SNc (Huddleston et al., 2018; Snyder and Connor, 2009). These bimodal concentrations have also been seen to change with the progression of Parkinson's Disease (PD), in which the loss of dopaminergic neurons and neuromelanin concentrations have been observed in SNc histology (Fearnley and Lees, 1991), whereas iron deposition is increased in both of the substantia nigra pars during pathological progression (Dexter et al., 1992). Although these biomarkers are observed with histological staining, histological staining is only done post-mortem to confirm diagnoses of Parkinsonian disorders Visualizing changes in the substantia nigra pars using non-invasive techniques could lead to clinically relevant biomarkers used to identify and diagnose early stages of disease or monitor disease pathology.

T_2-weighted (Gupta et al., 2010; Péran et al., 2007), T_1-weighted (Menke et al., 2010), and neuromelanin-sensitive (Sasaki et al., 2006) contrasts from structural magnetic resonance imaging (MRI) have been used to monitor global neural changes of parkinsonian pathology and distinguish between SNc and SNR. However, many studies utilize inconsistent divisions of the substantia nigra volume and use different regions of interest. In particular, substantia nigra from T_2-weighted and neuromelanin-sensitive contrasts have been shown to be spatially incongruent (Langley et al., 2015). This incongruence has led to inconsistencies in placement of regions of interest for SNc

and reduced reproducibility of results from previous studies examining pathology of parkinsonian disorders (Huddleston et al., 2018; Langley et al., 2019).

Current MRI contrasts used to delineate SNc and SNr have included susceptibility weighted imaging (SWI), R_2* mapping, and neuromelanin sensitive contrasts. Diffusion tensor imaging (DTI)-based tractography can also be used to parcellate SNc and SNr. DTI measures the movement of molecular water (Beaulieu, 2002) and can be used to measure the degree of restricted diffusion (fractional anisotropy, FA). DTI measures are sensitive to altered microstructural "integrity" (e.g., degeneration or demyelination), particularly in highly aligned white matter. As white matter consists of myelinated axons, the principle direction of of diffusion, calculated from from DTI data, can be used to reconstruct white matter tracts in DTI data using a procedure called DTI tractography.

A study parcellated the substantia nigra by utilizing T_1-mapping in combination with DTI-based tractography to map out various connections associated with each of the substantia nigra subregions(Menke et al., 2010). The study found tracts originating from SNc passed through the posterior striatum, the globus pallidus, and anterior thalamic nuclei then terminated in the prefrontal cortex, whereas tracts found within a separate portion of the posterior striatum and ventral thalamic nuclei which terminated in the sensorimotor cortices had voxels originating in the mask designated as SNr.

However, in a separate study utilizing post hoc spectral clustering of the connectivity patterns deduced from DTI-based tractography, Zhang and colleagues(Zhang et al., 2017) found a tripartite segmentation of the substantia nigra, which includes a dorsoventral segment, a dorsolateral segment, and a dorsomedial segment of the whole substantia nigral volume. Using these three segments, it was found that the dorsoventral segment showed higher connectivity to

the prefrontal cortex, the anterior cingulate cortex, and the anterior cortex, whereas the dorsolateral segment was found to show higher connectivity to the somatic motor and sensory cortices. In addition, the dorsomedial segment showed higher connectivity to orbitofrontal cortex and various regions within the limbic system, including the hippocampus and the amygdala.

While these regions show possible consistencies with previous work on the substantia nigra as a bilateral volume, with Zhang et al.'s dorsoventral segment being associated with the SNc and the dorsolateral segment being associated with the SNr, the third segmentation of the substantia nigra (the dorsomedial segment) produces a separate connectivity profile including both regions previously associated with the SNc, such as the orbitofrontal cortices, and regions associated with the SNr, such as portions of the limbic connections.

In this preliminary study, we attempt to delineate the connectivity between regions of the substantia nigra using DTI-based tractography. This study is the first part of an overall generalization of the substantia nigra pars divisions using T_2-weighted and neuromelanin-sensitive imaging, in which the results from this study will aid in the transformation of substantia nigral masks used in the following analyses. We hypothesize that the connectivity-maps produced by DTI-based tractography will show regioselectivity in their connections with their target masks, in which the SNc will prefer higher connectivity towards the posterior striatum as compared to the anterior striatum, and that the SNr will prefer higher connectivity towards the thalamic regions as compared to SNc connectivity in that same region.

Methods

Dataset

Five subjects from HCP S900 were utilized in this study (three female, two male, ages 26-35) (Van Essen et al., 2013).

DTI image preprocessing

Preprocessing was performed with the minimal preprocessing pipelines specified by HCP. Data processed using ICA-FIX was considered registered and used in the subsequent processing steps (Griffanti et al., 2014).

Standard preprocessing procedures were used to correct for various distortions, included susceptibility induced distortions in the diffusion MR data following the method of as performed by Anderson and colleagues (Andersson et al., 2003) with eddy current corrections using FSL software. Using the parameters derived from the diffusion MR data, such as fractional anisotropy (FA) were estimated. For each individual subject, the FA map was transformed to the T_1-weighted image. Following this transformation, no discernable difference was observed between the T_1-weighted image and the susceptibility distortion corrected diffusion data.

Generation of substantia nigra seed masks

The SN used in this study was segmented using a procedure outlined by Langley and colleagues (Langley et al., 2015). These masks were transformed into common MNI space using the FLIRT and FNIRT tools in the FSL software package in the following pipeline: first, brain extracted images from the T_1-weighted MP-RAGE sequence were aligned with the brain extracted MNI-152 image using affine transformation (Smith et al., 2004; Woolrich et al., 2009); next, a

nonlinear transformation (using the FNIRT tool) was used to generate a transformation between individual subject space and common space. An overlap region consisting of 10% of the SNc volume was drawn between the border between the SNc and SNr after the initial segmentation. Finally, each individual SN mask was transformed to their respective T_1-weighted image using FLIRT and then transformed to common space. After the transformation of each SN mask into the common MNI space, the SN masks were thresholded at a level of 0.6 and binarized for subsequent DTI-based tractography. Finally, the SN masks were transformed back into subject space and used as seed masks for the DTI connectivity analyses.

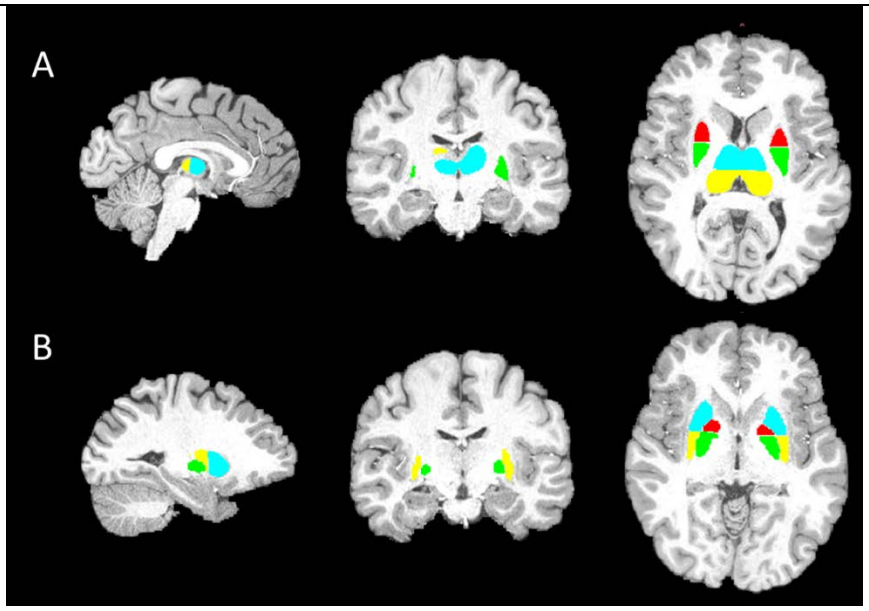

Figure 1: **A)** Target masks for the anterior striatum (red), posterior striatum (green), anterior thalamus (light blue), and posterior thalamus (yellow). **B)** Target masks for the anterior globus pallidus (red), Posterior globus pallidus (green), anterior putamen (light blue), posterior putamen (yellow). All masks were transformed into subject space, binarized, and thresholded to 0.6 for use in DTI-based tractography.

Fiber tracking

Prior to fiber tracking, brain extraction and white matter masks were created from the anatomical scans using BET (Smith, 2002) and FAST (Zhang et al., 2001) in the FSL software package (Smith et al., 2004; Woolrich et al., 2009). Probabilistic tractography, implemented using FSL, was used to track the fiber tracts originating from the three SN volumes. We used four regions separated by both the anterior and posterior regions, totaling eight target masks (*Figure 1*). The procedure to generate seed masks and target masks were as follows: All target masks were taken from the Harvard-Oxford atlas (http://fsl.fmrib.ox.ac.uk/fsl/fslwiki/atlases) and transformed to each subject's T_1 space using a rigid body transformation.

For each subject, probabilistic tractography was carried out from all voxels in each seed mask for both hemisphere using a model accommodating two fiber orientations (Behrens et al., 2007). Probability density functions were calculated by drawing 5,000 samples from the uncertainty distribution of the fiber orientations between the seed masks and the cortical target masks. The number of these samples reached the target mask was counted as the waytotal. After each subject's 5,000 tracts were tracked, the pathways were normalized by the waytotal number, and the normalized value in each voxel was interpreted as the tract probability given the prior knowledge that the tract exists in that voxel. Then, each subject's tract probabilities were transformed to MNI space using a nonlinear transformation.

Statistical Analyses

Data comparisons were grouped into two groups of two regions with the three substantia nigra volumes: striatum versus thalamus connectivity and globus pallidus versus putamen connectivity. To determine statistically significant normalized tract pairings, single-factor

ANOVA was performed on each of the two data sets from each of the substantia nigra-target mask pairings with a 5 degrees of freedom between groups, 24 degrees of freedom within groups, α-value set at 0.05, and an F-critical value at 2.6206. To determine significant pairwise comparisons, Tukey's HSD test was performed for each pair, with a q-critical set at 4.38.

Results

Representative tractography results for each of the target masks from a representative subject are shown in *Figures 2-7*, with the image thresholded to the 90% of the tracts represented as a heat map. Each figure represents a pairing between the substantia nigra regions (SNc, SNr, and overlap regions) and the target masks (anterior/posterior striatum, anterior/posterior thalamus, anterior/posterior globus pallidus, and anterior/posterior putamen), represented in subject space.

Box and whisker plots from each of the two groups and their pairwise comparisons are shown for each of the subjects for each target mask (*Figure 8 & 9*). In addition, Single-Factor ANOVA showed significant results in all four target masks (F-critical = 2.6206, $F > 2.6206$, $p < 0.05$). However, subsequent Tukey's HSD test revealed only significant differences between SNc connectivities versus SNr and overlap connections ($Q > 4.38$), whereas connectivities between SNr and overlap regions were not significantly different than each other for all target masks. ($Q < 4.38$). Regioselective comparisons between Anterior and posterior segments did not show significant differences for all substantia nigra pars regions and target masks ($Q < 4.38$).

From these comparisons, SNc connectivity was determined to be significantly different between SNr and overlap regions but were not shown to be statistically significant between anterior versus posterior. SNr and overlap connectivity were not statistically significant to both each other and between their anterior versus posterior counterparts for all the target volumes.

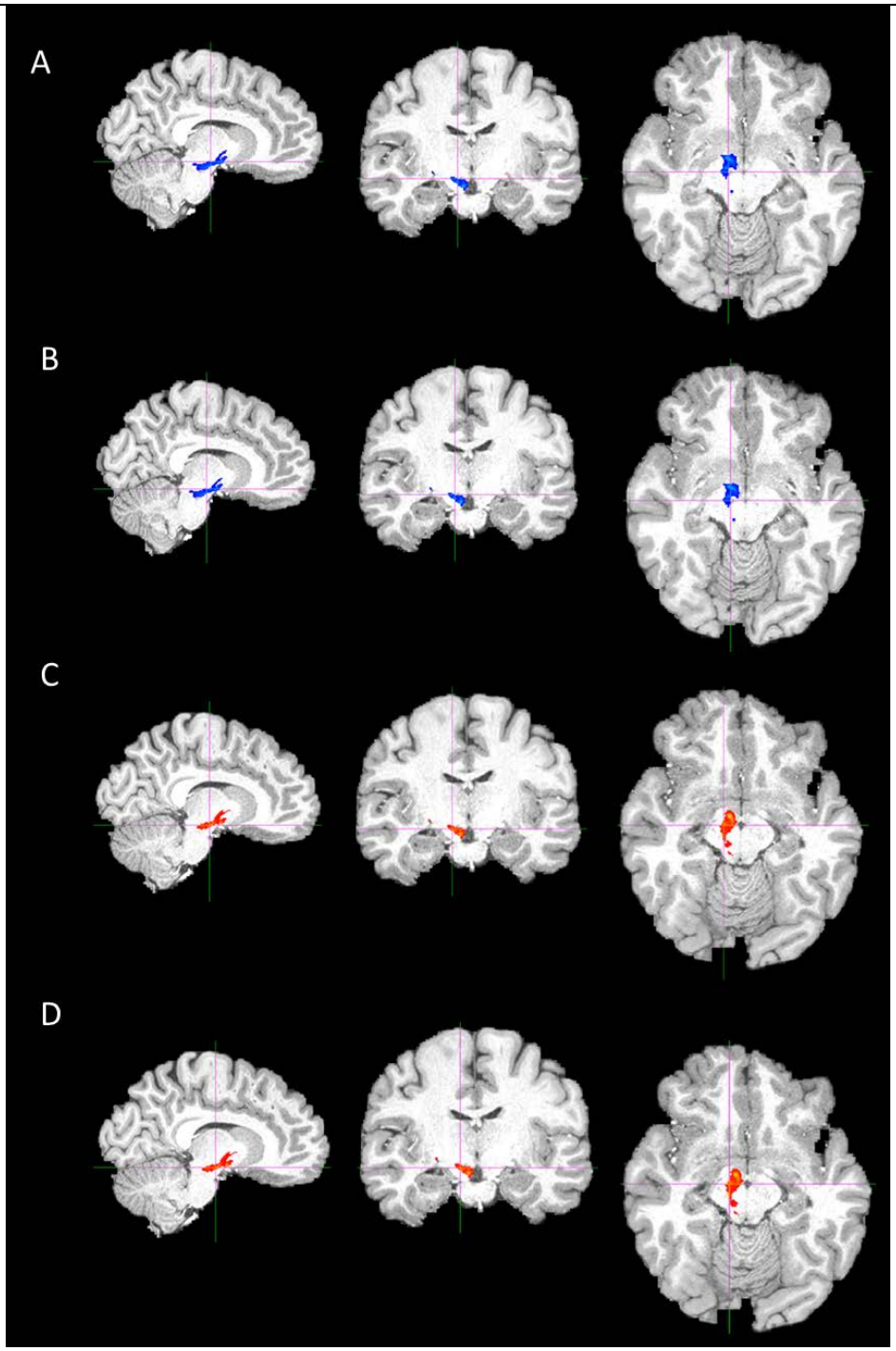

Figure 2: Probabilistic Tracking between the SNc and the target masks from a representative subject. Picture thresholded to remove lower 10% of tracts. **A)** SNc tracts to anterior striatum, **B)** SNc tracts to posterior striatum, **C)** SNc tracts to anterior thalamus, **D)** SNc tracts to posterior thalamus.

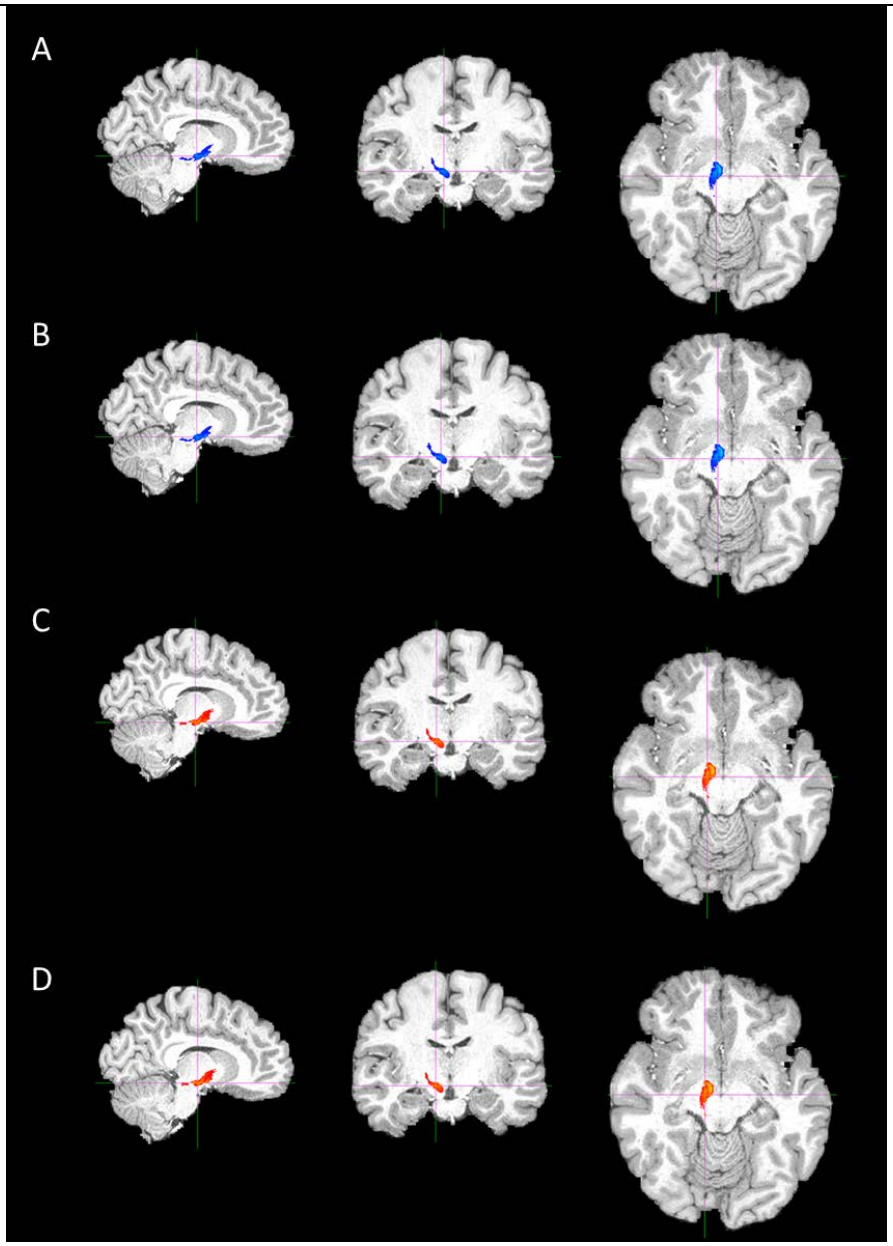

Figure 3: Probabilistic Tracking between the SNr and the target masks from a representative subject. Picture thresholded to remove lower 10% of tracts. **A)** SNr tracts to anterior striatum, **B)** SNr tracts to posterior striatum, **C)** SNr tracts to anterior thalamus, **D)** SNr tracts to posterior thalamus

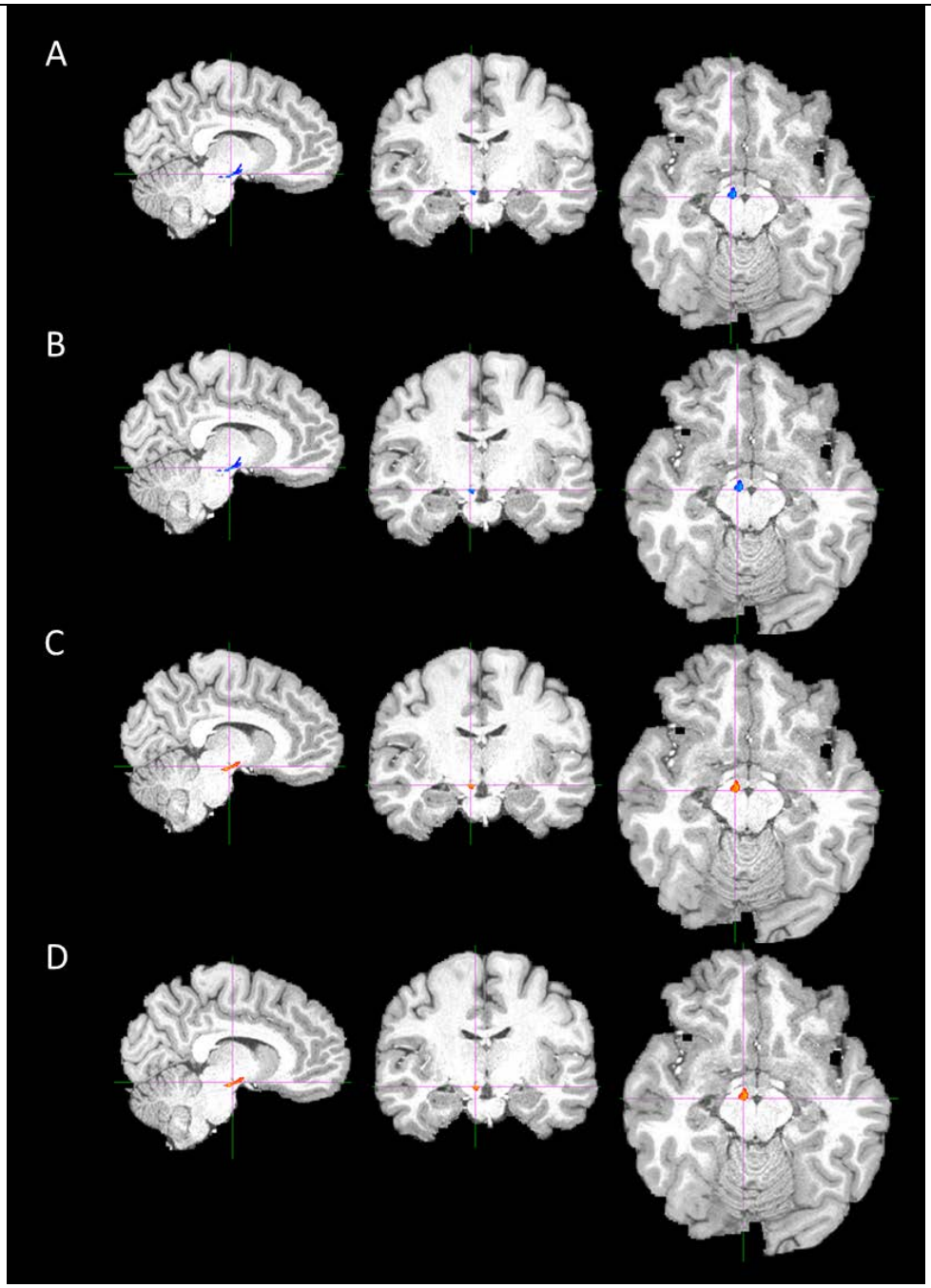

Figure 4: Probabilistic Tracking between the overlap region and the target masks from a representative subject. Picture thresholded to remove lower 10% of tracts. **A)** Overlap tracts to anterior striatum, **B)** Overlap tracts to posterior striatum, **C)** Overlap tracts to anterior thalamus, **D)** Overlap tracts to posterior thalamus

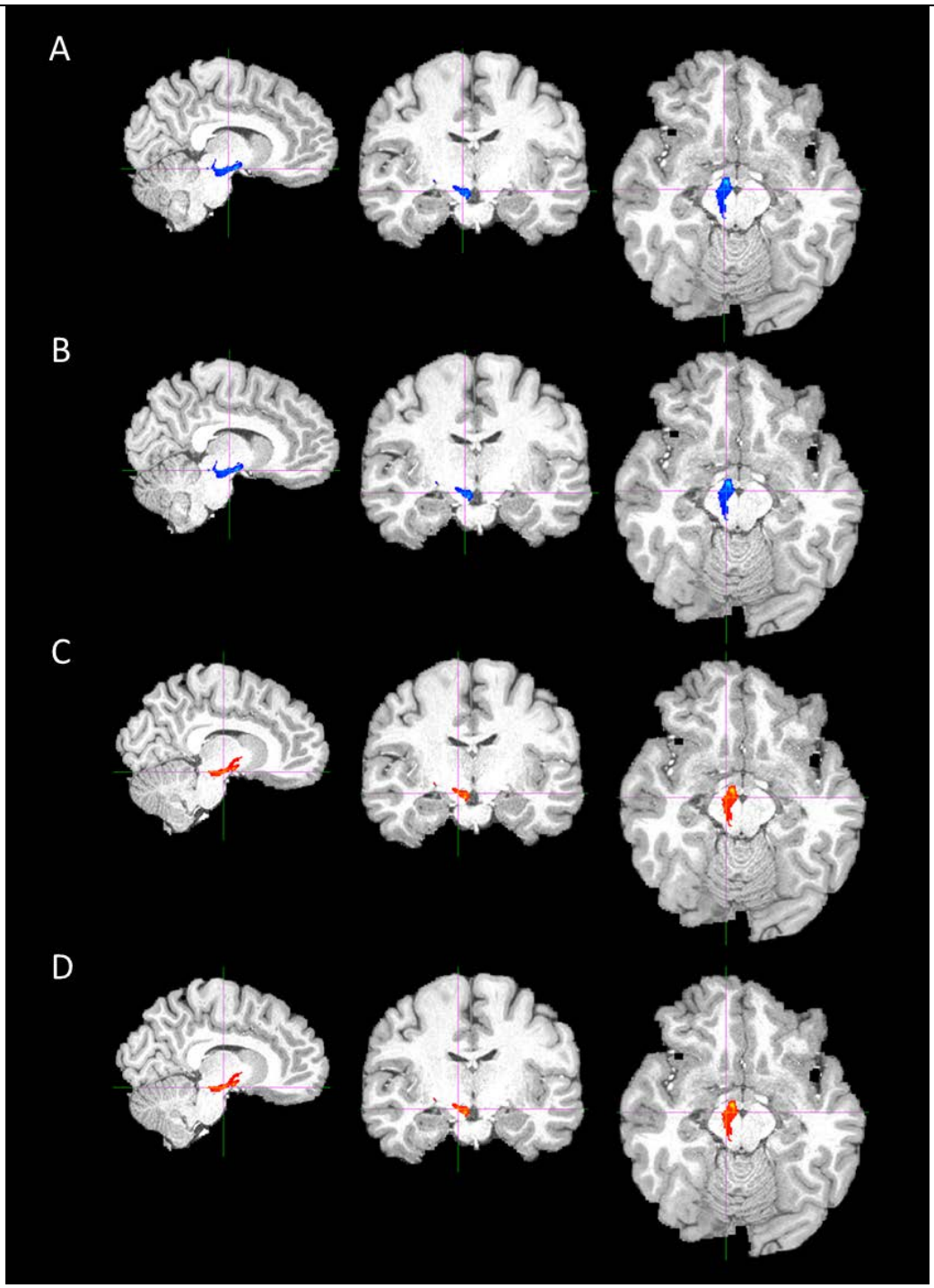

Figure 5: Probabilistic Tracking between the SNc and the target masks from a representative subject. Picture thresholded to remove lower 10% of tracts. **A)** SNc tracts to anterior globus pallidus, **B)** Overlap tracts to posterior globus pallidus, **C)** Overlap tracts to anterior putamen, **D)** Overlap tracts to posterior putamen

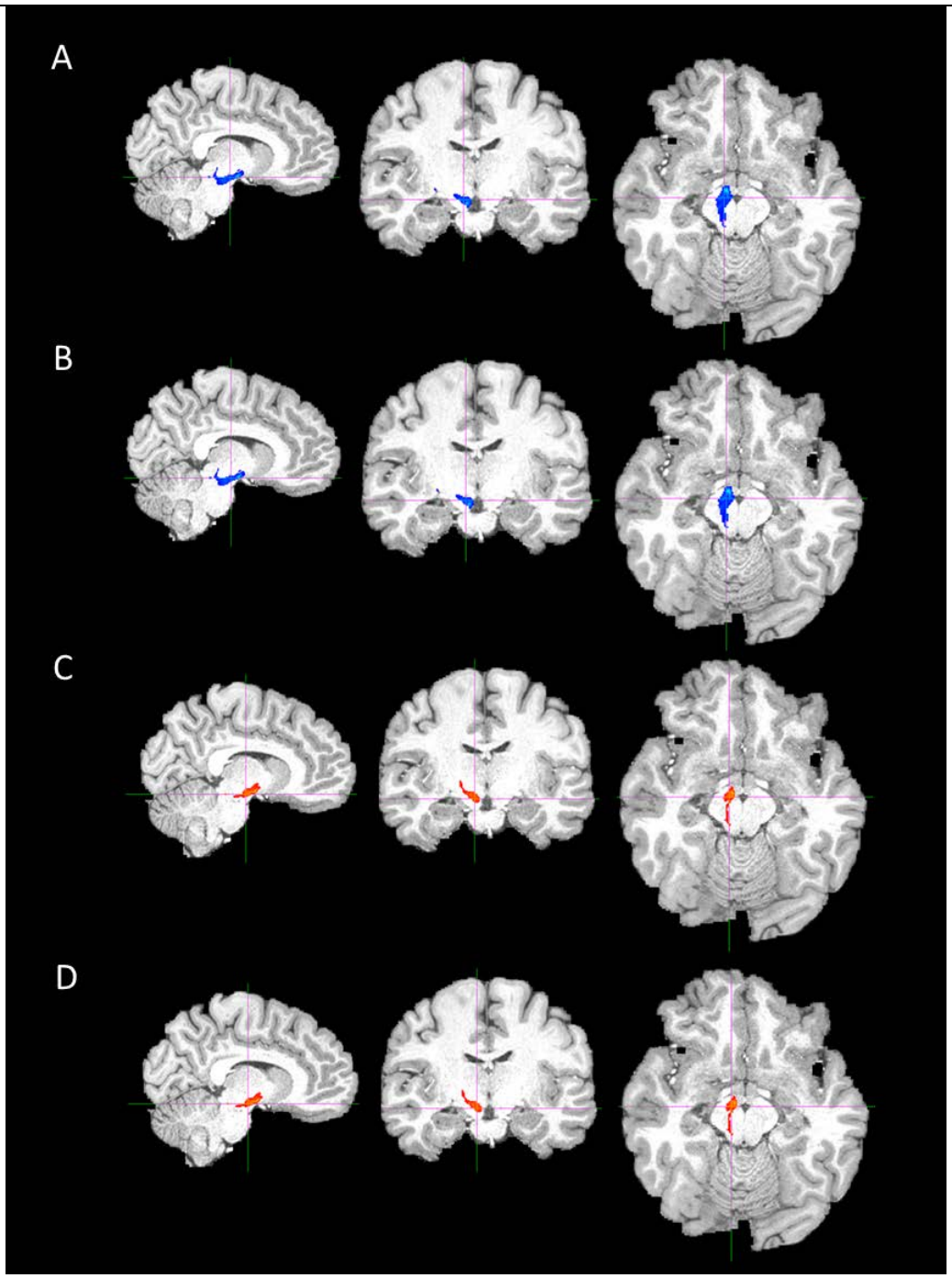

Figure 6: Probabilistic Tracking between the SNr and the target masks from a representative subject. Picture thresholded to remove lower 10% of tracts. **A)** SNr tracts to anterior globus pallidus, **B)** SNr tracts to posterior globus pallidus, **C)** SNr tracts to anterior putamen, **D)** SNr tracts to posterior putamen

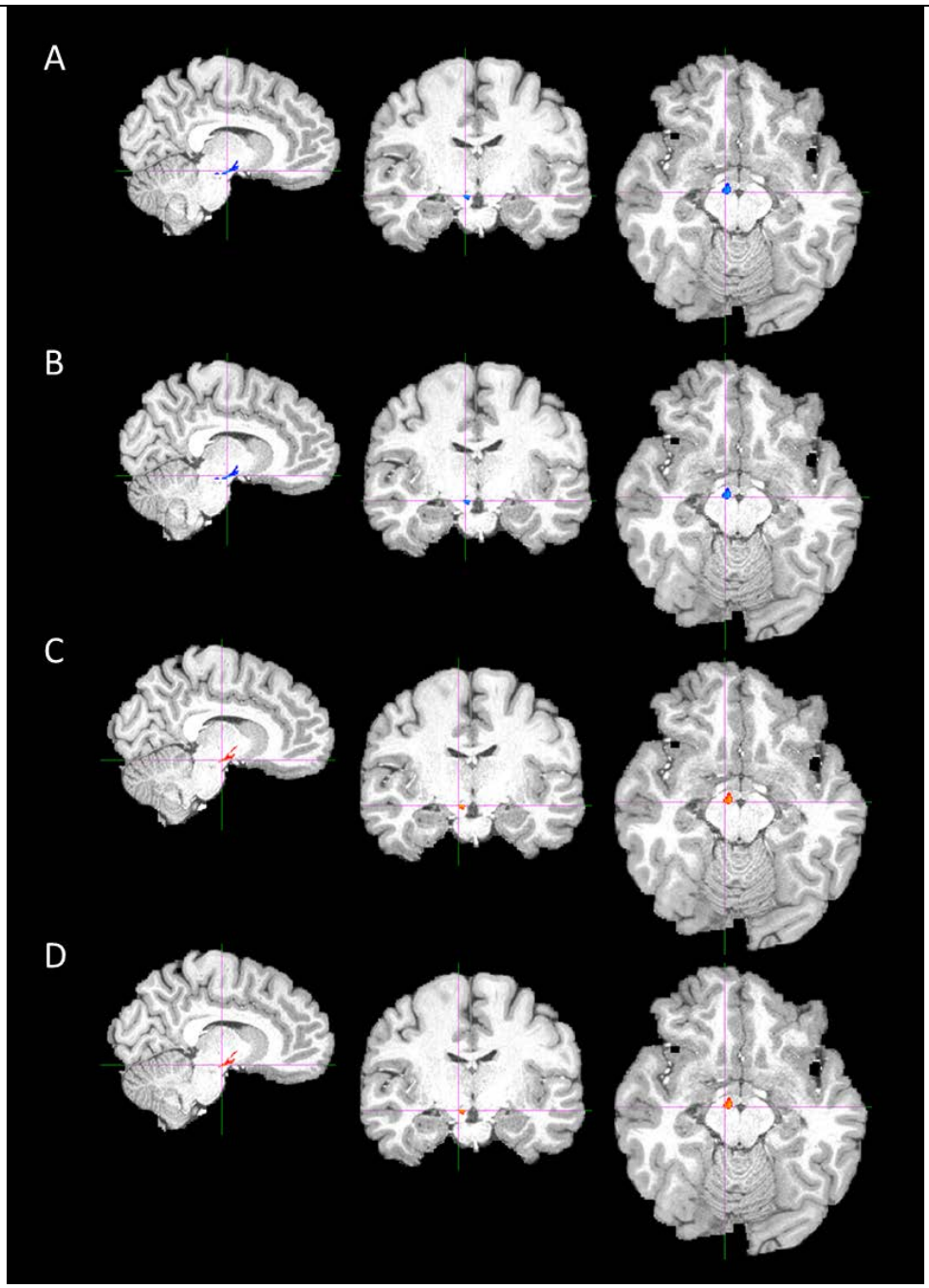

Figure 7: Probabilistic Tracking between the overlap region and the target masks from a representative subject. Picture thresholded to remove lower 10% of tracts. **A)** Overlap tracts to anterior globus pallidus, **B)** Overlap tracts to posterior globus pallidus, **C)** Overlap tracts to anterior putamen, **D)** Overlap tracts to posterior putamen

A)

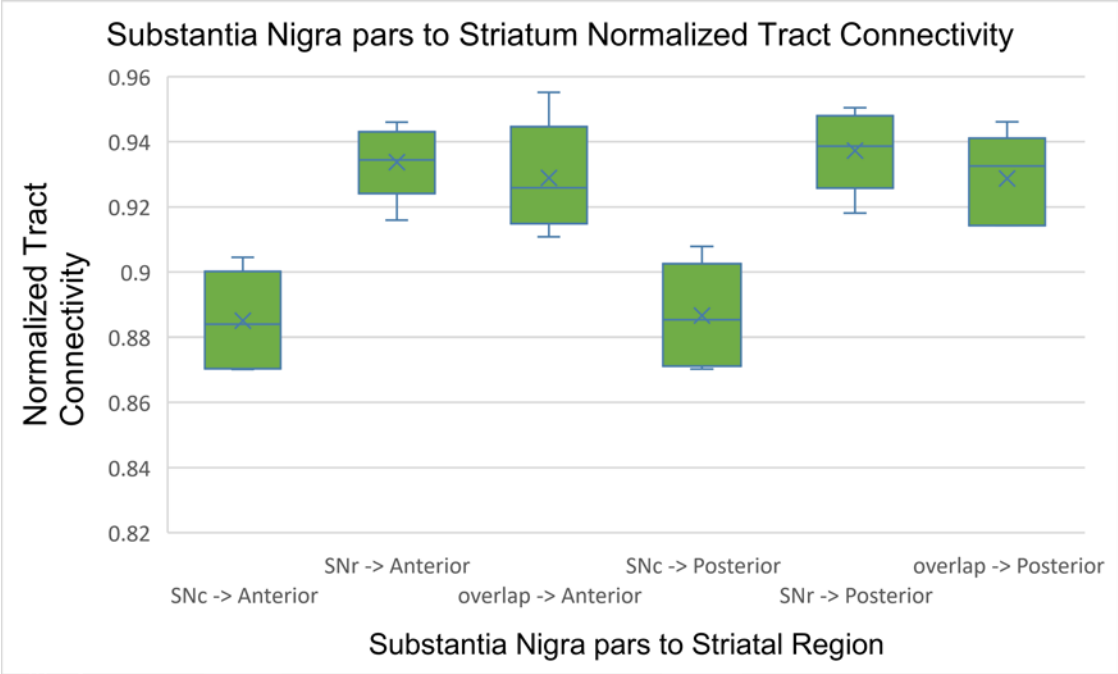

B)

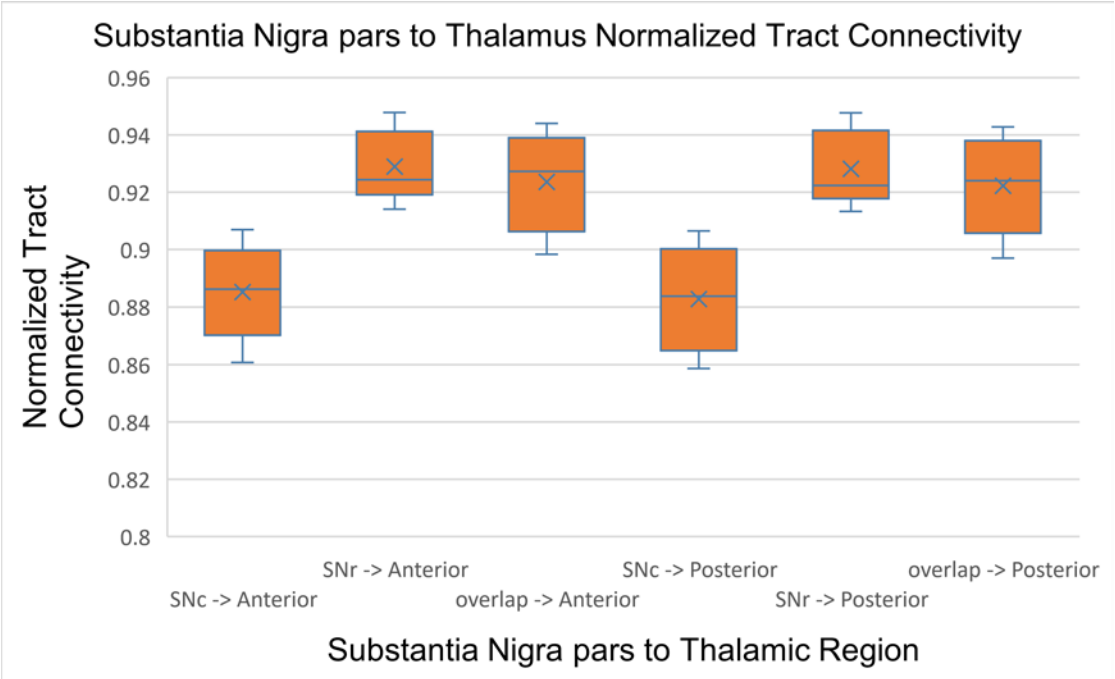

Figure 8: Box and Whisker plots of each of the substantia nigra pars to **A)** Anterior and Posterior Striatal regions and **B)** Anterior and Posterior Thalamic regions.

A)

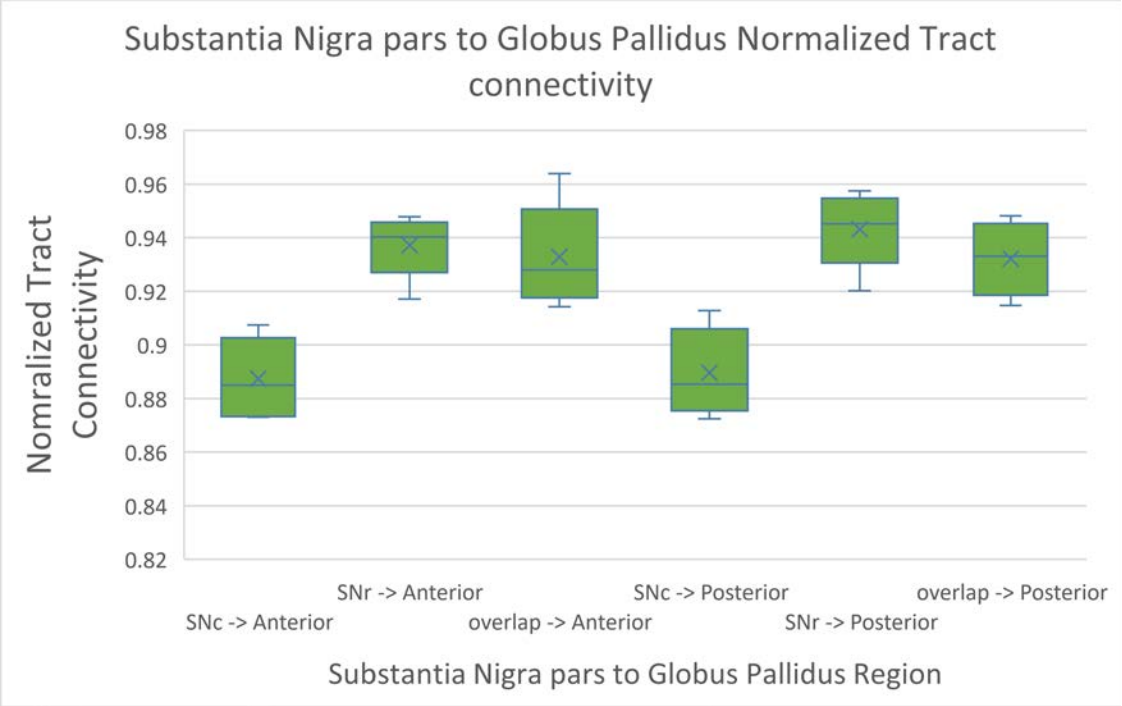

B)

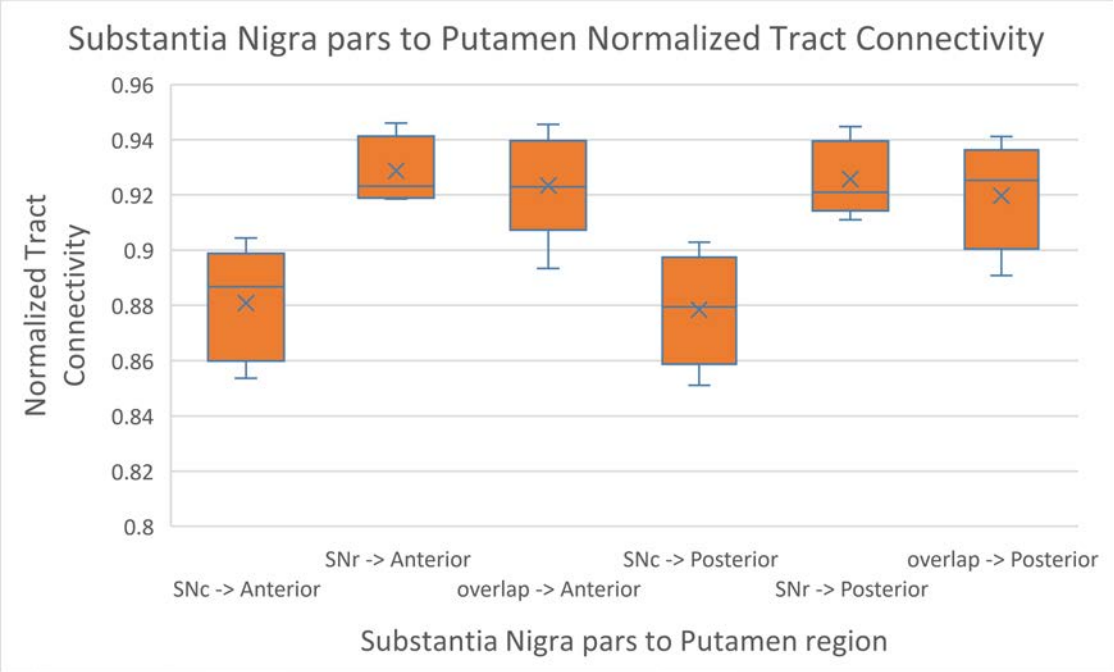

Figure 9: Box and Whisker plots of each of the substantia nigra pars to **A)** Anterior and Posterior Globus Pallidus regions and **B)** Anterior and Posterior Putamen regions.

Discussion

From the present study between the differences in normalized connectivity in substantia nigra pars and target masks between various regions, several significant results were obtained. In all of the target regions, namely the striatum, thalamus, globus pallidus, and putamen, SNc connectivity in both anterior and posterior segmentations of the target mask were shown to be significantly different than both the SNr connections and the overlap ($F > 2.6024$, $p < 0.05$ for all target masks) and positive results from Tukey's HSD tests ($Q > 4.38$ for SNc and SNR/overlap pairs).

There were no significant differences between the SNr connectivity and the overlap connectivity, as shown by negative results from Tukey's HSD tests ($Q < 4.38$ for all tests between SNr and overlap regions). However, none of the target masks showed any significant differences between the anterior and posterior normalized connectivity. This result was also the same in other substantia nigra pars regions including the SNc, SNr, and the overlap region, as anterior and posterior tracts were not able to delineate the various connections between the two ($Q < 4.38$).

While these results have not proven a successful delineation of structural connectivity differences between SNc and SNr, the non-significant differences between the overlap region and the SNr region may indicate a significant portion of those voxels within the overlap region to be a majority if not entirely consisting of neurons originating from the SNr region. While it cannot be visually inspected from connectivity maps, especially since many tracts within the brain regions presented in this study overlap with each other, the difference in contours and normalized connectivity at least shows a difference in tracts emanating from SNc and SNr. Because the overlap normalized connectivity closely matches and is significantly higher than the SNc normalized connectivity, this could be the beginning of the nigrostriatal tract and the tracts from SNc and SNr

are bundled within the tract. This may make it impossible to differentiate between the two regions terminating in the striatum alone. Future studies should use the striatum and thalamus as waypoints to the frontal and motor cortices to further differentiate between two nigral regions.

Another portion of the study that also remained non-significant in the single-factor ANOVA and subsequent Tukey's HSD testing was the regioselectivity of the connections either through the anterior or posterior portion of each of the target masks ($Q < 4.38$ for regioselective pairs). This non-significant result may be because concentrations of tracts may be closely bound in the nigrostriatal tract and separation of their projections may require additional targets in the motor and frontal cortexes to sufficiently separate the fibers.

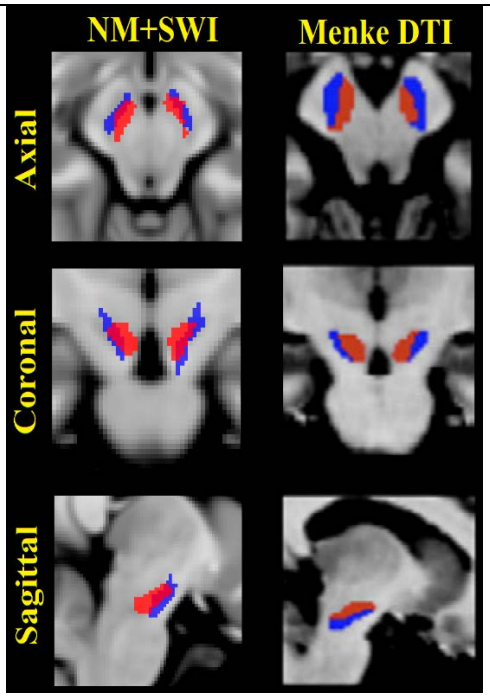

Figure 10: Differences in substantia nigra masks used in in this work (Langley et al., 2015) and Menke et al. in 2010 (Menke et al., 2010), respectively. The NM-MRI SN and T2/SWI SN are shown in red and blue, respectively, in the first column. The second column shows masks from

Menke, et al. In the second column, the SNc (internal) compartment is shown in red, whereas SNr (external) compartments is shown in blue.

In a previous study by Menke and colleagues (Menke et al., 2010), a similar segmentation of the substantia nigra was used for fiber tracking (*Figure 10*). While our substantia nigra masks are similar to Menke et al.'s substantia nigra mask, their fiber tracking analysis used the striatum and thalamus as waypoints for target masks in the cortex. Our analyses only utilized the striatum and the thalamus as target masks only, which may account for the differences in results between the present study and these earlier findings. We hypothesize that this inclusion of tracking towards the cortex may allow for more separation between the tracts and replicate these earlier findings. In addition, the use of T_2*-weighted imaging has already been shown to produce different segmentations of the substantia nigra volumes as compared to a neuromelanin-based approach to segmentation (Huddleston et al., 2018; Langley et al., 2019). From an initial study using structural images and a following DTI-based tractography, these results at least support a portion of delineation of the two pars in healthy controls.

Conclusion

While this study failed to show significant differences between regioselectivity and the connectivity between the overlap region with the SNr, a significant difference is shown between the SNc and the other pars segmentations applied to the tractography. This difference significantly showed in each of the target masks, from the striatum to the putamen, that the SNc consistently showed lower normalized connectivity between the target masks as compared to both the SNr and overlap regions. However, this non-significant result between the different regions of the same

anatomical structure may be due to the overgeneralized and wide area of projection not segmented by the anterior and posterior portions of each structure. Furthermore, the non-significant result from between SNr and overlap segments of the substantia nigra may show that the overlap region contains a majority of neurons associated with the SNr, and that further segmentation and study is needed to better segment this overlap region. Overall, this study serves as preliminary data to a larger study on the delineation of the substantia nigra using various imaging and statistical methods, which will eventually use both susceptibility-weighted imaging and neuromelanin-sensitive based tractography.

References

Andersson, J.L.R., Skare, S., Ashburner, J., 2003. How to correct susceptibility distortions in spin-echo echo-planar images: Application to diffusion tensor imaging. Neuroimage 20, 870–888. https://doi.org/10.1016/S1053-8119(03)00336-7

Beaulieu, C., 2002. The basis of anisotropic water diffusion in the nervous system - A technical review. NMR Biomed. https://doi.org/10.1002/nbm.782

Behrens, T.E.J., Berg, H.J., Jbabdi, S., Rushworth, M.F.S., Woolrich, M.W., 2007. Probabilistic diffusion tractography with multiple fibre orientations: What can we gain? Neuroimage 34, 144–155. https://doi.org/10.1016/j.neuroimage.2006.09.018

Dexter, D.T., Jenner, P., Schapira, A.H.V., Marsden, C.D., 1992. Alterations in levels of iron, ferritin, and other trace metals in neurodegenerative diseases affecting the basal ganglia. Ann. Neurol. 32, S94–S100. https://doi.org/10.1002/ana.410320716

Fearnley, J.M., Lees, A.J., 1991. Ageing and Parkinson's Disease: Substantia Nigra Regional Selectivity, Brain.

Griffanti, L., Salimi-Khorshidi, G., Beckmann, C.F., Auerbach, E.J., Douaud, G., Sexton, C.E., Zsoldos, E., Ebmeier, K.P., Filippini, N., Mackay, C.E., Moeller, S., Xu, J., Yacoub, E., Baselli, G., Ugurbil, K., Miller, K.L., Smith, S.M., 2014. ICA-based artefact removal and accelerated fMRI acquisition for improved resting state network imaging. Neuroimage 95, 232–247. https://doi.org/10.1016/j.neuroimage.2014.03.034

Gupta, D., Saini, J., Kesavadas, C., Sarma, P.S., Kishore, A., 2010. Utility of susceptibility-weighted MRI in differentiating Parkinson's disease and atypical parkinsonism. Neuroradiology 52, 1087–1094. https://doi.org/10.1007/s00234-010-0677-6

Huddleston, D.E., Langley, J., Dusek, P., He, N., Faraco, C.C., Crosson, B., Factor, S., Hu, X.P.,

2018. Imaging Parkinsonian Pathology in Substantia Nigra with MRI. Curr. Radiol. Rep. https://doi.org/10.1007/s40134-018-0272-x

Langley, J., He, N., Huddleston, D.E., Chen, S., Yan, F., Crosson, B., Factor, S., Hu, X., 2019. Reproducible detection of nigral iron deposition in 2 Parkinson's disease cohorts. Mov. Disord. 34, 416–419. https://doi.org/10.1002/mds.27608

Langley, J., Huddleston, D.E., Chen, X., Sedlacik, J., Zachariah, N., Hu, X., 2015. A multicontrast approach for comprehensive imaging of substantia nigra. Neuroimage 112, 7–13. https://doi.org/10.1016/j.neuroimage.2015.02.045

Menke, R.A., Jbabdi, S., Miller, K.L., Matthews, P.M., Zarei, M., 2010. Connectivity-based segmentation of the substantia nigra in human and its implications in Parkinson's disease. Neuroimage 52, 1175–1180. https://doi.org/10.1016/j.neuroimage.2010.05.086

Péran, P., Hagberg, G., Luccichenti, G., Cherubini, A., Brainovich, V., Celsis, P., Caltagirone, C., Sabatini, U., 2007. Voxel-based analysis of R2* maps in the healthy human brain. J. Magn. Reson. Imaging 26, 1413–1420. https://doi.org/10.1002/jmri.21204

Sasaki, M., Shibata, E., Tohyama, K., Takahashi, J., Otsuka, K., Tsuchiya, K., Takahashi, S., Ehara, S., Terayama, Y., Sakai, A., 2006. Neuromelanin magnetic resonance imaging of locus ceruleus and substantia nigra in Parkinson's disease. Neuroreport 17, 1215–1218. https://doi.org/10.1097/01.wnr.0000227984.84927.a7

Smith, S.M., 2002. Fast robust automated brain extraction. Hum. Brain Mapp. 17, 143–155. https://doi.org/10.1002/hbm.10062

Smith, S.M., Jenkinson, M., Woolrich, M.W., Beckmann, C.F., Behrens, T.E.J., Johansen-Berg, H., Bannister, P.R., De Luca, M., Drobnjak, I., Flitney, D.E., Niazy, R.K., Saunders, J., Vickers, J., Zhang, Y., De Stefano, N., Brady, J.M., Matthews, P.M., 2004. Advances in

Functional and Structural MR Image Analysis and Implementation as FSL Technical Report TR04SS2.

Snyder, A.M., Connor, J.R., 2009. Iron, the substantia nigra and related neurological disorders. Biochim. Biophys. Acta - Gen. Subj. https://doi.org/10.1016/j.bbagen.2008.08.005

Van Essen, D.C., Smith, S.M., Barch, D.M., Behrens, T.E.J., Yacoub, E., Ugurbil, K., 2013. The WU-Minn Human Connectome Project: An overview. Neuroimage 80, 62–79. https://doi.org/10.1016/j.neuroimage.2013.05.041

Woolrich, M.W., Jbabdi, S., Patenaude, B., Chappell, M., Makni, S., Behrens, T., Beckmann, C., Jenkinson, M., Smith, S.M., 2009. Bayesian analysis of neuroimaging data in FSL. Neuroimage 45. https://doi.org/10.1016/j.neuroimage.2008.10.055

Zhang, Y., Brady, M., Smith, S., 2001. Segmentation of brain MR images through a hidden Markov random field model and the expectation-maximization algorithm. IEEE Trans. Med. Imaging 20, 45–57. https://doi.org/10.1109/42.906424

Zhang, Y., Larcher, K.M.-H., Misic, B., Dagher, A., 2017. Anatomical and functional organization of the human substantia nigra and its connections. Elife 6. https://doi.org/10.7554/eLife.26653